

Recent neutrino oscillation result with the IceCube experiment

The IceCube Collaboration

(a complete list of authors can be found at the end of the proceedings)

E-mail: shiqiyu@icecube.wisc.edu

The IceCube South Pole Neutrino Observatory is a Cherenkov detector instrumented in a cubic kilometer of ice at the South Pole. IceCube's primary scientific goal is the detection of TeV neutrino emissions from astrophysical sources. At the lower center of the IceCube array, there is a subdetector called DeepCore, which has a denser configuration that makes it possible to lower the energy threshold of IceCube and observe GeV-scale neutrinos, opening the window to atmospheric neutrino oscillations studies. Advances in physics sensitivity have recently been achieved by employing Convolutional Neural Networks to reconstruct neutrino interactions in the DeepCore detector. In this contribution, the recent IceCube result from the atmospheric muon neutrino disappearance analysis using the CNN-reconstructed neutrino sample is presented and compared to the existing worldwide measurements.

Corresponding authors: Shiqi Yu^{1*}, Jessie Micallef^{2,3}

¹ *Michigan State University*

² *Massachusetts Institute of Technology*

³ *Tufts University*

* Presenter

The 38th International Cosmic Ray Conference (ICRC2023)
26 July – 3 August, 2023
Nagoya, Japan



1. Introduction

Neutrinos are generated and detected as three flavors, namely $\nu_{e,\mu,\tau}$ via weak interactions, while they propagate in their mass eigenstates: $\nu_{1,2,3}$. However, as they travel, they propagate in their respective mass eigenstates, denoted as $\nu_{1,2,3}$. Due to their non-zero masses, the flavor observed in the detection of a neutrino may differ from its original flavor upon creation. This phenomenon is called neutrino oscillation. Neutrinos oscillations have been observed and studied by many experiments [1–6]. The probability of being created in one flavor and subsequently detected in another is described by a unitary matrix, the Pontecorvo-Maki-Nakagawa-Sakata (PMNS) [7] matrix. This unitary matrix can be parameterized by three mixing angles (θ_{12} , θ_{13} , and θ_{23}), one CP-violating phase δ_{CP} , and the squared mass differences, $\Delta m_{ij}^2 \equiv m_i^2 - m_j^2$, between the three neutrino masses m_i , where $i, j = 1, 2, 3$. In this study, we measure the values of Δm_{32}^2 and θ_{23} via the ν_μ disappearance channel by studying atmospheric muon neutrinos with the IceCube Neutrino Observatory. For the other oscillation parameters that are previously well measured, we employ the reported values by [8] ($\Delta m_{21}^2 \approx 7.4 \times 10^{-5} \text{eV}^2/c^4$, $\theta_{13} \approx 9^\circ$, and $\theta_{12} \approx 34^\circ$).

The spectrum of cosmic rays at Earth follows a power-law with an isotropic distribution. This generates an atmospheric neutrino flux that also follows a power-law for all zenith angles. In this analysis, we make use of the energy of the neutrino, E , and the distance from their generation point to the detector, L , which can be parametrized as a function of the zenith angle, θ_{zenith} .

Atmospheric muon neutrinos are produced by the hadronic processes of cosmic rays interacting with matter in the atmosphere. The interaction spreads all over the atmosphere at all energy ranges, which provides a rich muon neutrino sample with broad ranges of neutrino energy (E) and distance of travel (L). The existing long-baseline experiments have fixed baselines and narrowly peaked neutrino beam energies optimized for neutrino oscillation studies, while IceCube can use the highest L and E in the oscillation analysis. In the effective approximation of two-flavor oscillations, the ν_μ survival probability reads:

$$P(\nu_\mu \rightarrow \nu_\mu) \approx 1 - \sin^2(2\theta_{23}) \sin^2 \frac{1.27 \Delta m_{32}^2 L}{E}, \quad (1)$$

which depends on the distance traveled, L , and the neutrino energy E . The mixing angle of θ_{23} and mass splitting of Δm_{32}^2 are the parameters to be measured and are plotted against L (represented by arrival angle, θ_{zenith}) and E in Figure 1. The values of Δm_{32}^2 can affect the frequency of oscillation stripes (see Figure 1), and hence, the locations of the strips. The brightness of the stripes is affected by the value of θ_{23} , which corresponds to the amplitude in Equation 1. The sensitivities to these two oscillation parameters arise mainly from the neutrino sample arriving through the Earth ($\cos \theta_{zenith} \lesssim 0$) with energy between 5 and 100 GeV. Additionally, the first oscillation ‘‘dip’’, for example, near 30 GeV in Figure 1 with the underlying assumptions on the oscillation parameters, gives us a strong sensitivity to the Δm_{32}^2 value.

2. DeepCore Detector

The IceCube detector (see Figure 2) comprises 5,160 digital optical modules (DOMs) instrumenting a volume of over one km^3 of South Pole glacial ice deep below the surface. Each DOM contains a photomultiplier tube (PMT) and the associated electronics to detect and read out photons

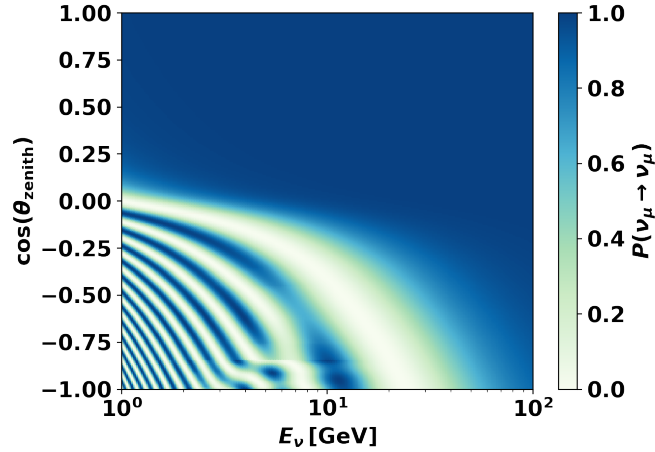


Figure 1: Distribution of ν_μ survival probability with color representing the value of probability at given values of $\cos(\theta_{\text{zenith}})$ and E with oscillation parameters from the previous result [9].

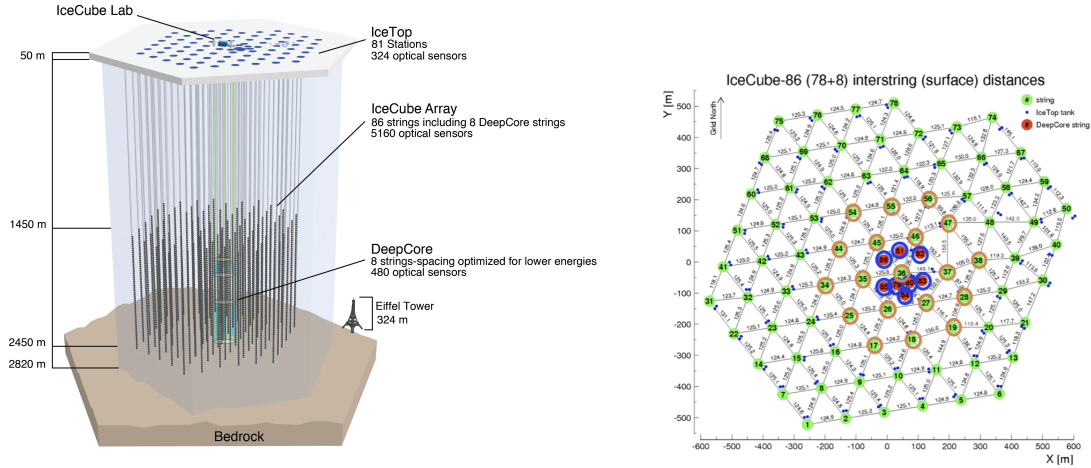


Figure 2: IceCube neutrino observatory's main in-ice array and DeepCore sub-detector (left) and surface layout of strings (right) where red-filled DeepCore strings and orange-circled IceCube main strings are used in the CNN reconstruction.

as electronic signals. These DOMs can detect Cherenkov photons produced by the relativistic charged particles propagating through the ice, produced initially by neutrino interactions within the detector, and convert these signals into digitized waveforms. The arrival photons' charge and time information can be extracted from the digitized waveforms and used as inputs to a Convolutional Neural Network (CNN) [10–12] for reconstructing neutrino interactions. The DeepCore sub-detector, located in the bottom center of the IceCube array (see left panel of Figure 2), and the surrounding IceCube strings of the main array (eight red-filled and 19 orange-circled green dots in the right panel of Figure 2) offer exceptional capabilities to reconstruct events in the sub-100 GeV energy range. The DeepCore detector has a denser instrumented volume of ice ($\sim 10^7$ m³) with higher quantum efficiency DOMs compared with those of the main array, which grants us the

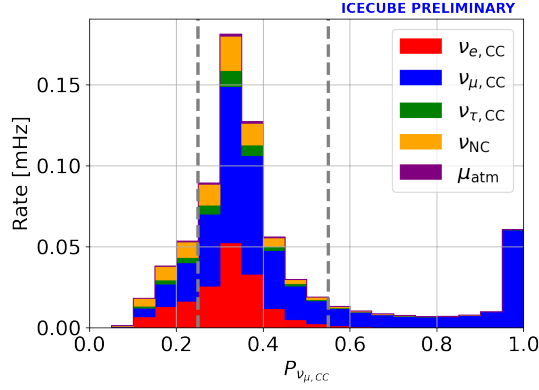


Figure 3: Stacked distributions of CNN-reconstructed PID with color representing different Monte Carlo (MC) components, dashed lines indicate boundaries between cascade- (left), mixed- (middle), and signal-like (right) events.

ability to study neutrinos with observed energy between 5 and 100 GeV arriving through the Earth (with $L \sim 1.3 \times 10^4$ km for those passing through the Earth core).

This analysis uses the data taken between 2012 and 2021, an equivalent livetime of 9.3 years. The simulation and calibration techniques are the same as the previous result [9], whereas machine-learning (ML) reconstruction techniques are developed and employed, and background-like neutrino candidates help to better constrain systematic uncertainties.

3. Reconstruction and Event Selection

We developed and applied the convolutional neural networks (CNNs) focused on the DeepCore sub-detector to reconstruct the sub-100 GeV neutrino sample, which contributes the most to the sensitivity of this study. With the help of CNN reconstructions, we select a final neutrino-rich sample with contamination from atmospheric muons well below 1% of the selected sample.

The training of CNNs is optimized separately for neutrino energy [10], arrival direction (θ_{zenith}) [11], interaction vertex position, particle identification (PID), and atmospheric muon classification [12]. We keep the neutrino candidates with their starting vertex close to DeepCore to ensure better reconstruction resolution. Energy and zenith cuts are applied to keep neutrinos with reconstructed energy between 5 and 100 GeV arriving from below the horizon, which is the region, as described in Section 1 and shown in Figure 1, that gives us the best sensitivity to oscillation parameter measurements. The CNN-reconstructed PID classifier (as shown in Figure 3) selects the signal-like candidates, i.e., ν_{μ} charged current (CC) interactions, over the background-like neutrino interactions (all remaining types) of this analysis. Signal-like events have a track-like topology in the detector because of their outgoing primary muons, while background-like events look like scattered cascades due to their electromagnetic and hadronic showers. A boosted decision tree is employed to serve as the atmospheric muon classifier, which helps to keep the final sample neutrino-dominated with the rate of atmospheric muon background events well within 0.6% of the sample.

The CNNs are trained independently using differently optimized samples to achieve optimized reconstruction performances on all variables. The neutrino energy and interaction vertex position

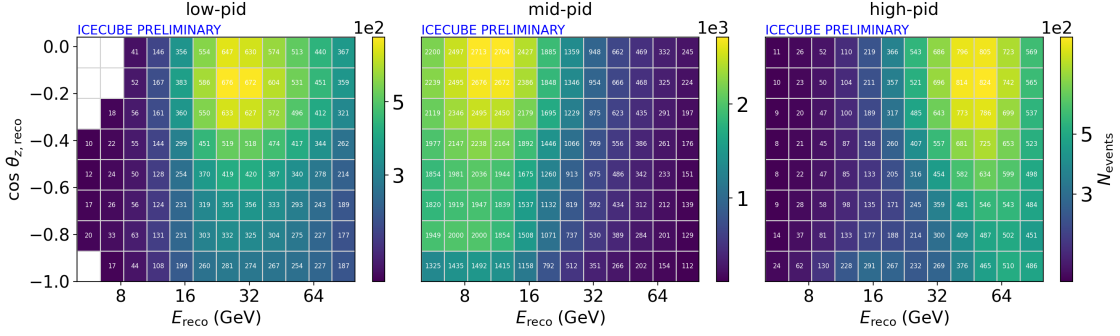


Figure 4: Selected analysis sample in bins of neutrino energy, zenith angle, and PID (cascade-, mixed-, and track-like samples from left to right). Blank bins are not used in the analysis due to their low MC statistics.

are trained on a ν_μ CC sample with a uniform energy spectrum between 1 and 300 GeV, with a tail extending to 500 GeV. The zenith angle, θ_{zenith} , is trained using ν_μ CC events starting and ending near DeepCore generated with a uniform true θ_{zenith} distribution. The PID identifier is trained on a sample with an equal number of track-like and cascade-like neutrino events. The atmospheric muon classifier is trained on a balanced sample of track-like and cascade-like neutrino interactions and atmospheric muons. All the DOMs on the 8 DeepCore and surrounding 19 IceCube strings, as shown in Figure 2, are incorporated to the CNN via two separate input layers due to their different spatial densities. With a similar performance to the state-of-the-art likelihood-based reconstructions [13], the most considerable improvement of using CNN is from the processing speed (approximately 3,000 times faster), which is a significant advantage considering the large statistics of the full MC production of atmospheric neutrino datasets used in these analyses.

4. Analysis

We bin the selected neutrino sample using 3D binning: reconstructed energy, $\cos(\theta_{\text{zenith}})$, and PID (see Figure 3). The high-PID bin ($\text{PID} \geq 0.55$) has the highest purity of signal-like events, while cascade-like events dominate the low-PID bin ($\text{PID} < 0.25$). The ten logarithmic energy bins and eight linear $\cos(\theta_{\text{zenith}})$ bins help to reveal the oscillation pattern in the low energy up-going region while not pushing beyond the limitation of reconstruction resolution. The binned analysis sample can be found in Figure 4.

The treatment of systematic uncertainties follow a similar procedure of the previous analysis. [9]. In this analysis, the list of free parameters is decided by re-evaluating their impacts on the recovery of the true underlying physics parameters. The fitted values of the systematic parameters compared to their nominal values and prior ranges and shown in Figure 5. We employ neutrino interaction cross-section uncertainties from GENIE 2.12.8 [14], except for the deep-inelastic scattering (DIS) parameter which is interpolated between GENIE and CSMS [15] for a higher energy range of coverage; uncertainties of atmospheric flux hadronic production are parameterized following the ‘‘Barr’’ parameters (‘‘Atm. flux Y/W/I/H/G’’) [16]; ‘‘Atm. flux $\Delta\gamma$ ’’ represents the uncertainty on the cosmic-ray spectral shape; ‘‘ N_{bfr} ’’ accounts for the difference in ice properties of employing the birefringent polycrystalline microstructure ice-model [17] and that of the nominal MC (SPICE

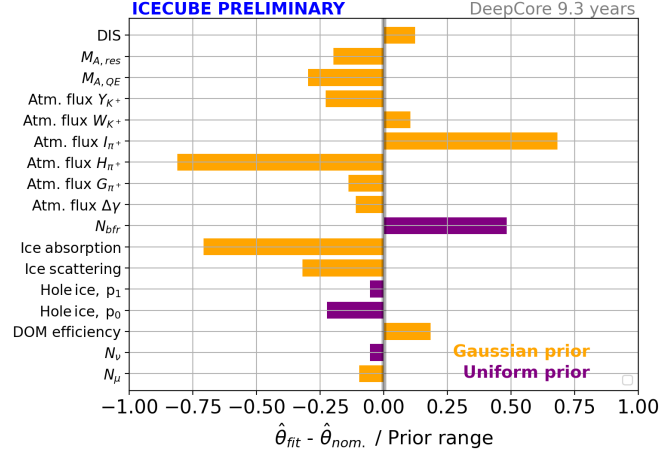


Figure 5: Fitted systematic uncertainty parameters pulled from nominal values compared to ranges of priors. Detailed descriptions and references of individual parameters are in the main text.

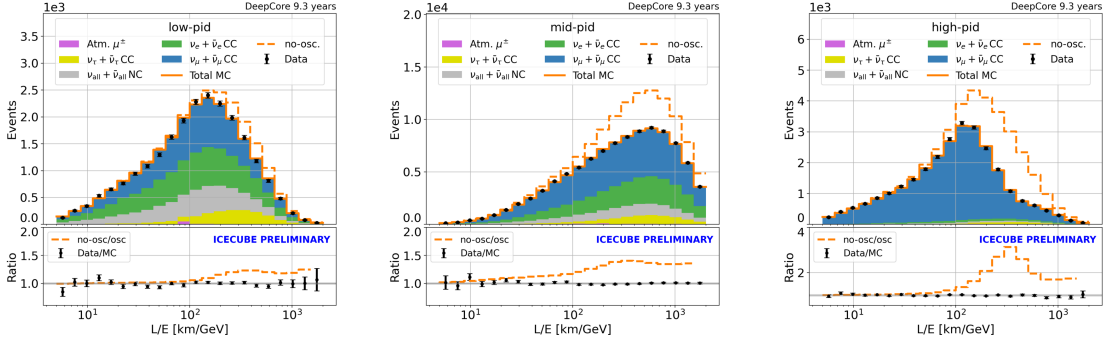


Figure 6: Data (black) and stacked MC comparisons of L/E projections with top panels showing events in cascade- (left), mixed- (middle), and track-like (right) bins with (solid) and without (dashed) muon neutrino disappearance applied, and bottom panels showing ratios of data/MC (black) and MC ratios of without/with oscillations (dashed orange).

3.2.1 [9]); single-DOM light efficiency, parameters affecting photon propagation in glacial ice (“ice absorption” and “ice scattering”), and refrozen ice in drilling holes (“Hole ice, $p_{0(1)}$ ”) have been introduced in the previous analysis [9]; and “ N_ν ” (“ N_μ ”) describes the uncertainty on the normalization of neutrino (muon) flux.

5. Result and Conclusion

After the final selections, the low-energy atmospheric neutrino dataset taken between 2012-2021 contains 150,257 events. We achieve a good data/MC agreement and a distinctive signature of muon neutrino disappearance in the track-like bin, as shown in Figure 6.

Figure 7 shows the 90% confidence level (C.L.) contours of $\sin^2(\theta_{23})$ and Δm_{32}^2 assuming neutrino masses are in normal ordering ($m_3 > m_2 > m_1$). This result is consistent with all the

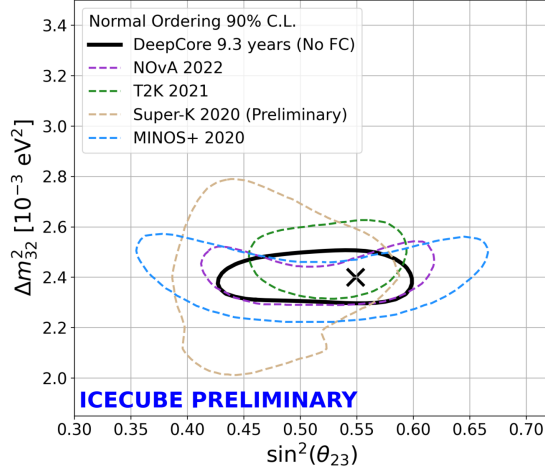


Figure 7: 90% C.L. contours (using Wilks’ theorem[18] and assuming normal mass ordering) and best-fit parameters (cross) of $\sin^2(\theta_{23})$ and Δm_{32}^2 compared to contours of other experiments [3–5, 19].

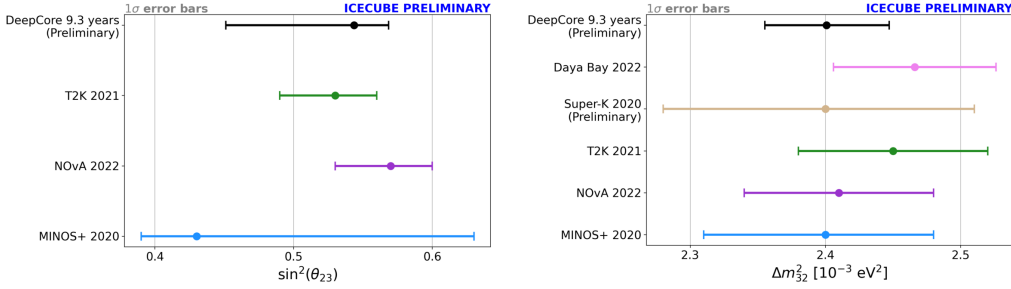


Figure 8: One σ uncertainties (using Wilks’ theorem and assuming normal mass ordering) on $\sin^2(\theta_{23})$ (left) and Δm_{32}^2 (right) of this result (black) compared with the existing measurements [3–6, 20].

previous accelerator and atmospheric neutrino oscillation measurements, as shown by the strong overlap in the 90% C.L. contours. Given the competitive sensitivity to the current world-leading measurements, improvements in the precision of global fits to neutrino oscillation parameters are expected once this result is incorporated. Since this analysis is sensitive to a higher energy range compared to other oscillations experiments and the detector technology is unique, it carries a distinct set of systematic uncertainties. The observed consistency is thus a strong validation of the standard three massive neutrino oscillation model.

As shown in Figure 8, the reported 1σ uncertainties on the values of $\sin^2(\theta_{23})$ and Δm_{32}^2 from different experiments are largely well agreed. The uncertainty of Δm_{32}^2 measurement from this analysis has a narrower uncertainty than the existing measurements. This is primarily benefited from the first oscillation “dip” in our 2D oscillation pattern, as discussed in Section 1 and shown in Figure 1, the location of which contributes most to the sensitivity of Δm_{32}^2 constraint. Meanwhile, it also benefited from the large-statistic of selected neutrino-rich final sample, improved detector calibration and MC models, and the new ML-based reconstruction techniques.

There is a lot of room for future improvements in muon neutrino disappearance measurement

using low-energy atmospheric data with IceCube DeepCore. The near-future IceCube Upgrade [21] will help to further improve our sensitivity to muon neutrino disappearance by improving detector calibration and event resolution. There are improved MC models underway, which better describe the properties of glacial ice and the composition of atmospheric fluxes and can potentially improve future analysis. There are also ongoing analyses that are benefited from the CNN reconstructions and selections, such as non-standard neutrino interaction measurement and neutrino mass ordering searches. The CNN method could also be adapted and applied to the IceCube Upgrade, further improving the precision of neutrino oscillation measurements.

References

- [1] The IceCube Collaboration, *Phys. Rev. D* **99**, 032007 (2019).
- [2] The IceCube Collaboration, *Phys. Rev. Lett.* **120**, 071801 (2018).
- [3] The NOvA Collaboration, *Phys. Rev. D* **106**, 032004 (2022).
- [4] The T2K Collaboration, *Phys. Rev. D* **103**, 112008 (2021).
- [5] The MINOS+ Collaboration, *Phys. Rev. Lett.* **125**, 131802 (2020).
- [6] The Daya Bay Collaboration, *Phys. Rev. Lett.* **161802**, 130 (2023)
- [7] Maki, Z.; Nakagawa, M.; Sakata, S. *Progress of Theoretical Physics* **28**, 5 (1962)
- [8] The Particle Data Group, *Prog. Theor. Exp. Phys* **2022**, 083C01 (2022).
- [9] The IceCube Collaboration, submitted to *Phys. Rev. D*, arXiv:2304.12236.
- [10] J. Micallef on behalf of the IceCube Collaboration, PoS ICRC2021 **1053**, (2021)
- [11] S. Yu on behalf of the IceCube Collaboration, PoS ICRC2021 **1054**, (2021)
- [12] S. Yu on behalf of the IceCube Collaboration, *NuFACT 2022 proceedings, submitted to Physical Sciences Forum*
- [13] The IceCube Collaboration, *Eur. Phys. J. C* **82**, 807 (2022).
- [14] C. Andreopoulos *et al*, *Nucl. Instrum. Methods A* **614**, 87–104 (2010).
- [15] A. Cooper-Sarkar, P. Mertsch, and S. Sarkar, *JHEP* **08**, 042 (2011).
- [16] G. Barr, T. Gaisser, S. Robbins, and T. Stanev, *Phys. Rev. D* **74**, 094009 (2006).
- [17] D. Chirkin and M. Rongen on behalf of the IceCube Collaboration, PoS **ICRC2019**, 854 (2020).
- [18] Wilks, Samuel S. *The Annals of Mathematical Statistics* **9**, 1 (1938)
- [19] V. Takhistov on behalf of the Super-Kamiokande Collaboration, PoS **ICHEP2020**, 181 (2021).
- [20] M. Gonchar on behalf of the JUNO collaboration, presentation at Nucleus-2022.
- [21] A. Ishihara on behalf of the IceCube Collaboration, PoS **ICRC2019**, 1031 (2021).

Full Author List: IceCube Collaboration

R. Abbasi¹⁷, M. Ackermann⁶³, J. Adams¹⁸, S. K. Agarwalla^{40, 64}, J. A. Aguilar¹², M. Ahlers²², J.M. Alameddine²³, N. M. Amin⁴⁴, K. Andeen⁴², G. Anton²⁶, C. Argüelles¹⁴, Y. Ashida⁵³, S. Athanasiadou⁶³, S. N. Axani⁴⁴, X. Bai⁵⁰, A. Balagopal V.⁴⁰, M. Baricevic⁴⁰, S. W. Barwick³⁰, V. Basu⁴⁰, R. Bay⁸, J. J. Beatty^{20, 21}, J. Becker Tjus^{11, 65}, J. Beise⁶¹, C. Bellenghi²⁷, C. Benning¹, S. BenZvi⁵², D. Berley¹⁹, E. Bernardini⁴⁸, D. Z. Besson³⁶, E. Blaufuss¹⁹, S. Blot⁶³, F. Bontempo³¹, J. Y. Book¹⁴, C. Boscolo Meneguolo⁴⁸, S. Böser⁴¹, O. Botner⁶¹, J. Böttcher¹, E. Bourbeau²², J. Braun⁴⁰, B. Brinson⁶, J. Brostean-Kaiser⁶³, R. T. Burley², R. S. Busse⁴³, D. Butterfield⁴⁰, M. A. Campana⁴⁹, K. Carloni¹⁴, E. G. Carnie-Bronca², S. Chattopadhyay^{40, 64}, N. Chau¹², C. Chen⁶, Z. Chen⁵⁵, D. Chirkin⁴⁰, S. Choi⁵⁶, B. A. Clark¹⁹, L. Classen⁴³, A. Coleman⁶¹, G. H. Collin¹⁵, A. Connolly^{20, 21}, J. M. Conrad¹⁵, P. Coppin¹³, P. Correa¹³, D. F. Cowen^{59, 60}, P. Dave⁶, C. De Clercq¹³, J. J. DeLaunay⁵⁸, D. Delgado¹⁴, S. Deng¹, K. Deoskar⁵⁴, A. Desai⁴⁰, P. Desati⁴⁰, K. D. de Vries¹³, G. de Wasseige³⁷, T. DeYoung²⁴, A. Diaz¹⁵, J. C. Díaz-Vélez⁴⁰, M. Dittmer⁴³, A. Domi²⁶, H. Dujmovic⁴⁰, M. A. DuVernois⁴⁰, T. Ehrhardt⁴¹, P. Eller²⁷, E. Ellinger⁶², S. El Mentawi¹, D. Elsässer²³, R. Engel^{31, 32}, H. Erpenbeck⁴⁰, J. Evans¹⁹, P. A. Evenson⁴⁴, K. L. Fan¹⁹, K. Fang⁴⁰, K. Farrag¹⁶, A. R. Fazley⁷, A. Fedynitch⁵⁷, N. Feigl¹⁰, S. Fiedlschuster²⁶, C. Finley⁵⁴, L. Fischer⁴⁰, D. Fox⁵⁹, A. Franckowiak¹¹, A. Fritz⁴¹, P. Fürst¹, J. Gallagher³⁹, E. Ganster¹, A. Garcia¹⁴, L. Gerhardt⁹, A. Ghadimi⁵⁸, C. Glaser⁶¹, T. Glauch²⁷, T. Glüsenskamp^{26, 61}, N. Goehle³², J. G. Gonzalez⁴⁴, S. Goswami⁵⁸, D. Grant²⁴, S. J. Gray¹⁹, O. Gries¹, S. Griffin⁴⁰, S. Griswold⁵², K. M. Groth²², C. Günther¹, P. Gutjahr²³, C. Haack²⁶, A. Hallgren⁶¹, R. Halliday²⁴, L. Halve¹, F. Halzen⁴⁰, H. Hamdaoui⁵⁵, M. Ha Minh²⁷, K. Hanson⁴⁰, J. Hardin¹⁵, A. A. Harnisch²⁴, P. Hatch³³, A. Haungs³¹, K. Helbing⁶², J. Hellrung¹¹, F. Henningsen²⁷, L. Heuermann¹, N. Heyer⁶¹, S. Hickford⁶², A. Hidvegi⁵⁴, C. Hill¹⁶, G. C. Hill², K. D. Hoffman¹⁹, S. Hori⁴⁰, K. Hoshina^{40, 66}, W. Hou³¹, T. Huber³¹, K. Hultqvist⁵⁴, M. Hünnefeld²³, R. Hussain⁴⁰, K. Hymon²³, S. In⁵⁶, A. Ishihara¹⁶, M. Jacquart⁴⁰, O. Janik¹, M. Jansson⁵⁴, G. S. Japaridze⁵, M. Jeong⁵⁶, M. Jin¹⁴, B. J. P. Jones⁴, D. Kang³¹, W. Kang⁵⁶, X. Kang⁴⁹, A. Kappes⁴³, D. Kappesser⁴¹, L. Kardum²³, T. Karg⁶³, M. Karle²⁷, A. Karle⁴⁰, U. Katz²⁶, M. Kauer⁴⁰, J. L. Kelley⁴⁰, A. Khatee Zathul⁴⁰, A. Kheirandish^{34, 35}, J. Kiryluk⁵⁵, S. R. Klein^{8, 9}, A. Kochocki²⁴, R. Koirala⁴⁴, H. Kolanoski¹⁰, T. Kontrimas²⁷, L. Köpke⁴¹, C. Kopper²⁶, D. J. Koskinen²², P. Koundal³¹, M. Kovacevich⁴⁹, M. Kowalski^{10, 63}, T. Kozynets²², J. Krishnamoorthi^{40, 64}, K. Kruiswijk³⁷, E. Krupczak²⁴, A. Kumar⁶³, E. Kun¹¹, N. Kurahashi⁴⁹, N. Lad⁶³, C. Lagunas Gualda⁶³, M. Lamoureux³⁷, M. J. Larson¹⁹, S. Latseva¹, F. Lauber⁶², J. P. Lazar^{14, 40}, J. W. Lee⁵⁶, K. Leonard DeHolton⁶⁰, A. Leszczyńska⁴⁴, M. Lincetto¹¹, Q. R. Liu⁴⁰, M. Liubarska²⁵, E. Lohfink⁴¹, C. Love⁴⁹, C. J. Lozano Mariscal⁴³, L. Lu⁴⁰, F. Lucarelli²⁸, W. Luszczyk^{20, 21}, Y. Lyu^{8, 9}, J. Madsen⁴⁰, K. B. M. Mahn²⁴, Y. Makino⁴⁰, E. Manao²⁷, S. Mancina^{40, 48}, W. Marie Sainte⁴⁰, I. C. Mariş¹², S. Marka⁴⁶, Z. Marka⁴⁶, M. Marsee⁵⁸, I. Martinez-Soler¹⁴, R. Maruyama⁴⁵, F. Mayhew²⁴, T. McElroy²⁵, F. McNally³⁸, J. V. Mead²², K. Meagher⁴⁰, S. Mechbal⁶³, A. Medina²¹, M. Meier¹⁶, Y. Merckx¹³, L. Merten¹¹, J. Micallef²⁴, J. Mitchell⁷, T. Montaruli²⁸, R. W. Moore²⁵, Y. Morii¹⁶, R. Morse⁴⁰, M. Moulai⁴⁰, T. Mukherjee³¹, R. Naab⁶³, R. Nagai¹⁶, M. Nakos⁴⁰, U. Naumann⁶², J. Necker⁶³, A. Negi⁴, M. Neumann⁴³, H. Niederhausen²⁴, M. U. Nisa²⁴, A. Noell¹, A. Novikov⁴⁴, S. C. Nowicki²⁴, A. Obertacke Pollmann¹⁶, V. O'Dell⁴⁰, M. Oehler³¹, B. Oeyen²⁹, A. Olivas¹⁹, R. Ørsøe²⁷, J. Osborn⁴⁰, E. O'Sullivan⁶¹, H. Pandya⁴⁴, N. Park³³, G. K. Parker⁴, E. N. Paudel⁴⁴, L. Paul^{42, 50}, C. Pérez de los Heros⁶¹, J. Peterson⁴⁰, S. Philippen¹, A. Pizzuto⁴⁰, M. Plum⁵⁰, A. Pontén⁶¹, Y. Popovych⁴¹, M. Prado Rodriguez⁴⁰, B. Pries²⁴, R. Procter-Murphy¹⁹, G. T. Przybylski⁹, C. Raab³⁷, J. Rack-Helleis⁴¹, K. Rawlins³, Z. Rechav⁴⁰, A. Rehman⁴⁴, P. Reichherzer¹¹, G. Renzi¹², E. Resconi²⁷, S. Reusch⁶³, W. Rhode²³, B. Riedel⁴⁰, A. Rifaie¹, E. J. Roberts², S. Robertson^{8, 9}, S. Rodan⁵⁶, G. Roellinghoff⁵⁶, M. Rongen²⁶, C. Rott^{53, 56}, T. Ruhe²³, L. Ruohan²⁷, D. Rychbosch²⁹, I. Safa^{14, 40}, J. Saffer³², D. Salazar-Gallegos²⁴, P. Sampathkumar³¹, S. E. Sanchez Herrera²⁴, A. Sandrock⁶², M. Santander⁵⁸, S. Sarkar²⁵, S. Sarkar⁴⁷, J. Savelberg¹, P. Savina⁴⁰, M. Schaufel¹, H. Schieler³¹, S. Schindler²⁶, L. Schlickmann¹, B. Schlüter⁴³, F. Schlüter¹², N. Schmeisser⁶², T. Schmidt¹⁹, J. Schneider²⁶, F. G. Schröder^{31, 44}, L. Schumacher²⁶, G. Schwefer¹, S. Sclafani¹⁹, D. Seckel⁴⁴, M. Seikh³⁶, S. Seunarine⁵¹, R. Shah⁴⁹, A. Sharma⁶¹, S. Shefali³², N. Shimizu¹⁶, M. Silva⁴⁰, B. Skrzypek¹⁴, B. Smithers⁴, R. Snihur⁴⁰, J. Soedingrekso²³, A. Sogaard²², D. Soldin³², P. Soldin¹, G. Sommani¹¹, C. Spannfellner²⁷, G. M. Spiczak⁵¹, C. Spiering⁶³, M. Stamatikos²¹, T. Stanev⁴⁴, T. Stetzelberger⁹, T. Stürwald⁶², T. Stuttard²², G. W. Sullivan¹⁹, I. Taboada⁶, S. Ter-Antonyan⁷, M. Thiesmeyer¹, W. G. Thompson¹⁴, J. Thwaites⁴⁰, S. Tilav⁴⁴, K. Tollefson²⁴, C. Tönnis⁵⁶, S. Toscano¹², D. Tosi⁴⁰, A. Trettin⁶³, C. F. Tung⁶, R. Turcotte³¹, J. P. Twagirayezu²⁴, B. Ty⁴⁰, M. A. Unland Elorrieta⁴³, A. K. Upadhyay^{40, 64}, K. Upshaw⁷, N. Valtonen-Mattila⁶¹, J. Vandenbroucke⁴⁰, N. van Eijndhoven¹³, D. Vannerom¹⁵, J. van Santen⁶³, J. Vara⁴³, J. Veitch-Michaelis⁴⁰, M. Venugopal³¹, M. Vereecken³⁷, S. Verpoest⁴⁴, D. Veske⁴⁶, A. Vijai¹⁹, C. Walck⁵⁴, C. Weaver²⁴, P. Weigel¹⁵, A. Weindl³¹, J. Weldert⁶⁰, C. Wendt⁴⁰, J. Werthebach²³, M. Weyrauch³¹, N. Whitehorn²⁴, C. H. Wiebusch¹, N. Willey²⁴, D. R. Williams⁵⁸, J. Willison²⁴, L. Witthaus²³, A. Wolf¹, M. Wolf²⁷, G. Wrede²⁶, X. W. Xu⁷, J. P. Yanez²⁵, E. Yildizci⁴⁰, S. Yoshida¹⁶, R. Young³⁶, F. Yu¹⁴, S. Yu²⁴, T. Yuan⁴⁰, Z. Zhang⁵⁵, P. Zhelnin¹⁴, M. Zimmerman⁴⁰

¹ III. Physikalisches Institut, RWTH Aachen University, D-52056 Aachen, Germany

² Department of Physics, University of Adelaide, Adelaide, 5005, Australia

³ Dept. of Physics and Astronomy, University of Alaska Anchorage, 3211 Providence Dr., Anchorage, AK 99508, USA

⁴ Dept. of Physics, University of Texas at Arlington, 502 Yates St., Science Hall Rm 108, Box 19059, Arlington, TX 76019, USA

⁵ CTSPS, Clark-Atlanta University, Atlanta, GA 30314, USA

⁶ School of Physics and Center for Relativistic Astrophysics, Georgia Institute of Technology, Atlanta, GA 30332, USA

⁷ Dept. of Physics, Southern University, Baton Rouge, LA 70813, USA

⁸ Dept. of Physics, University of California, Berkeley, CA 94720, USA

⁹ Lawrence Berkeley National Laboratory, Berkeley, CA 94720, USA

¹⁰ Institut für Physik, Humboldt-Universität zu Berlin, D-12489 Berlin, Germany

¹¹ Fakultät für Physik & Astronomie, Ruhr-Universität Bochum, D-44780 Bochum, Germany

¹² Université Libre de Bruxelles, Science Faculty CP230, B-1050 Brussels, Belgium

- ¹³ Vrije Universiteit Brussel (VUB), Dienst ELEM, B-1050 Brussels, Belgium
¹⁴ Department of Physics and Laboratory for Particle Physics and Cosmology, Harvard University, Cambridge, MA 02138, USA
¹⁵ Dept. of Physics, Massachusetts Institute of Technology, Cambridge, MA 02139, USA
¹⁶ Dept. of Physics and The International Center for Hadron Astrophysics, Chiba University, Chiba 263-8522, Japan
¹⁷ Department of Physics, Loyola University Chicago, Chicago, IL 60660, USA
¹⁸ Dept. of Physics and Astronomy, University of Canterbury, Private Bag 4800, Christchurch, New Zealand
¹⁹ Dept. of Physics, University of Maryland, College Park, MD 20742, USA
²⁰ Dept. of Astronomy, Ohio State University, Columbus, OH 43210, USA
²¹ Dept. of Physics and Center for Cosmology and Astro-Particle Physics, Ohio State University, Columbus, OH 43210, USA
²² Niels Bohr Institute, University of Copenhagen, DK-2100 Copenhagen, Denmark
²³ Dept. of Physics, TU Dortmund University, D-44221 Dortmund, Germany
²⁴ Dept. of Physics and Astronomy, Michigan State University, East Lansing, MI 48824, USA
²⁵ Dept. of Physics, University of Alberta, Edmonton, Alberta, Canada T6G 2E1
²⁶ Erlangen Centre for Astroparticle Physics, Friedrich-Alexander-Universität Erlangen-Nürnberg, D-91058 Erlangen, Germany
²⁷ Technical University of Munich, TUM School of Natural Sciences, Department of Physics, D-85748 Garching bei München, Germany
²⁸ Département de physique nucléaire et corpusculaire, Université de Genève, CH-1211 Genève, Switzerland
²⁹ Dept. of Physics and Astronomy, University of Gent, B-9000 Gent, Belgium
³⁰ Dept. of Physics and Astronomy, University of California, Irvine, CA 92697, USA
³¹ Karlsruhe Institute of Technology, Institute for Astroparticle Physics, D-76021 Karlsruhe, Germany
³² Karlsruhe Institute of Technology, Institute of Experimental Particle Physics, D-76021 Karlsruhe, Germany
³³ Dept. of Physics, Engineering Physics, and Astronomy, Queen's University, Kingston, ON K7L 3N6, Canada
³⁴ Department of Physics & Astronomy, University of Nevada, Las Vegas, NV, 89154, USA
³⁵ Nevada Center for Astrophysics, University of Nevada, Las Vegas, NV 89154, USA
³⁶ Dept. of Physics and Astronomy, University of Kansas, Lawrence, KS 66045, USA
³⁷ Centre for Cosmology, Particle Physics and Phenomenology - CP3, Université catholique de Louvain, Louvain-la-Neuve, Belgium
³⁸ Department of Physics, Mercer University, Macon, GA 31207-0001, USA
³⁹ Dept. of Astronomy, University of Wisconsin–Madison, Madison, WI 53706, USA
⁴⁰ Dept. of Physics and Wisconsin IceCube Particle Astrophysics Center, University of Wisconsin–Madison, Madison, WI 53706, USA
⁴¹ Institute of Physics, University of Mainz, Staudinger Weg 7, D-55099 Mainz, Germany
⁴² Department of Physics, Marquette University, Milwaukee, WI, 53201, USA
⁴³ Institut für Kernphysik, Westfälische Wilhelms-Universität Münster, D-48149 Münster, Germany
⁴⁴ Bartol Research Institute and Dept. of Physics and Astronomy, University of Delaware, Newark, DE 19716, USA
⁴⁵ Dept. of Physics, Yale University, New Haven, CT 06520, USA
⁴⁶ Columbia Astrophysics and Nevis Laboratories, Columbia University, New York, NY 10027, USA
⁴⁷ Dept. of Physics, University of Oxford, Parks Road, Oxford OX1 3PU, United Kingdom
⁴⁸ Dipartimento di Fisica e Astronomia Galileo Galilei, Università Degli Studi di Padova, 35122 Padova PD, Italy
⁴⁹ Dept. of Physics, Drexel University, 3141 Chestnut Street, Philadelphia, PA 19104, USA
⁵⁰ Physics Department, South Dakota School of Mines and Technology, Rapid City, SD 57701, USA
⁵¹ Dept. of Physics, University of Wisconsin, River Falls, WI 54022, USA
⁵² Dept. of Physics and Astronomy, University of Rochester, Rochester, NY 14627, USA
⁵³ Department of Physics and Astronomy, University of Utah, Salt Lake City, UT 84112, USA
⁵⁴ Oskar Klein Centre and Dept. of Physics, Stockholm University, SE-10691 Stockholm, Sweden
⁵⁵ Dept. of Physics and Astronomy, Stony Brook University, Stony Brook, NY 11794-3800, USA
⁵⁶ Dept. of Physics, Sungkyunkwan University, Suwon 16419, Korea
⁵⁷ Institute of Physics, Academia Sinica, Taipei, 11529, Taiwan
⁵⁸ Dept. of Physics and Astronomy, University of Alabama, Tuscaloosa, AL 35487, USA
⁵⁹ Dept. of Astronomy and Astrophysics, Pennsylvania State University, University Park, PA 16802, USA
⁶⁰ Dept. of Physics, Pennsylvania State University, University Park, PA 16802, USA
⁶¹ Dept. of Physics and Astronomy, Uppsala University, Box 516, S-75120 Uppsala, Sweden
⁶² Dept. of Physics, University of Wuppertal, D-42119 Wuppertal, Germany
⁶³ Deutsches Elektronen-Synchrotron DESY, Platanenallee 6, 15738 Zeuthen, Germany
⁶⁴ Institute of Physics, Sachivalaya Marg, Sainik School Post, Bhubaneswar 751005, India
⁶⁵ Department of Space, Earth and Environment, Chalmers University of Technology, 412 96 Gothenburg, Sweden
⁶⁶ Earthquake Research Institute, University of Tokyo, Bunkyo, Tokyo 113-0032, Japan

Acknowledgements

The authors gratefully acknowledge the support from the following agencies and institutions: USA – U.S. National Science Foundation-Office of Polar Programs, U.S. National Science Foundation-Physics Division, U.S. National Science Foundation-EPSCoR, Wisconsin Alumni Research Foundation, Center for High Throughput Computing (CHTC) at the University of Wisconsin–Madison, Open Science

Grid (OSG), Advanced Cyberinfrastructure Coordination Ecosystem: Services & Support (ACCESS), Frontera computing project at the Texas Advanced Computing Center, U.S. Department of Energy-National Energy Research Scientific Computing Center, Particle astrophysics research computing center at the University of Maryland, Institute for Cyber-Enabled Research at Michigan State University, and Astroparticle physics computational facility at Marquette University; Belgium – Funds for Scientific Research (FRS-FNRS and FWO), FWO Odysseus and Big Science programmes, and Belgian Federal Science Policy Office (Belspo); Germany – Bundesministerium für Bildung und Forschung (BMBF), Deutsche Forschungsgemeinschaft (DFG), Helmholtz Alliance for Astroparticle Physics (HAP), Initiative and Networking Fund of the Helmholtz Association, Deutsches Elektronen Synchrotron (DESY), and High Performance Computing cluster of the RWTH Aachen; Sweden – Swedish Research Council, Swedish Polar Research Secretariat, Swedish National Infrastructure for Computing (SNIC), and Knut and Alice Wallenberg Foundation; European Union – EGI Advanced Computing for research; Australia – Australian Research Council; Canada – Natural Sciences and Engineering Research Council of Canada, Calcul Québec, Compute Ontario, Canada Foundation for Innovation, WestGrid, and Compute Canada; Denmark – Villum Fonden, Carlsberg Foundation, and European Commission; New Zealand – Marsden Fund; Japan – Japan Society for Promotion of Science (JSPS) and Institute for Global Prominent Research (IGPR) of Chiba University; Korea – National Research Foundation of Korea (NRF); Switzerland – Swiss National Science Foundation (SNSF); United Kingdom – Department of Physics, University of Oxford.